Characterization of Electrical Conductivity of Anisotropic CFRP Materials by Means of Induction Thermography Technique

H.K. Bui, F. Senghor, Guillaume Wasselynck, Didier Trichet, J. Fouladgar, K. Lee, Gerard Berthiau

Characterization of Electrical Conductivity of Anisotropic CFRP Materials by Means of Induction Thermography Technique

H. K. Bui[1], F. D. Senghor[1], G. Wasselynck[1], D. Trichet[1], J. Fouladgar[1], K. Lee[2], and G. Berthiau[1]

[1]IREENA, University of Nantes, 44600 Saint-Nazaire, France
[2]Department of Physics, Sogang University, Seoul 121-742, South Korea

Numerical simulations by means of finite elements are used to investigate the capacities of the induction thermography technique for the characterization of electrical conductivities of unidirectional carbon fiber reinforced polymer (CFRP) materials. A coupled electromagnetic-thermal model is presented using hexahedral elements to deal with the thin region of fully anisotropic physical properties. Eddy-current problem is solved using the T-Ω formulation to deduce heat source density power. Transient thermal problem is solved with a fixed time step. An error minimization-based method is presented to identify the electrical resistivity of unidirectional CFRP from the induction thermography measurement.

***Index Terms*— Carbon fiber reinforced polymer (CFRP), coupled model, electrical conductivity characterization, induction thermography.**

materials have been widely used in aerospace to replace metals in structural components due to their lightweight and excellent and configurable mechanical properties.

Because of their conception, these materials have strong anisotropic physical properties. In terms of electrical conductivity, since carbon fibers are good conductors, CFRP composites have a good conductivity in the direction of carbon fibers but a very poor conductivity in perpendicular directions. The low conductivity may cause problems in practical applications, for example in induction welding of these materials or in electromagnetic shielding. The conductivities in different directions depend on the filling rate of carbon fibers, the manufacturing process, and also the presence of flaws.

The characterization of the electrical conductivities of CFRP helps to improve their properties. In the literature, some non-contact techniques based on electromagnetic effects have been proposed to characterize the electrical conductivities of this kind of material. Eddy-current methods are classical ones with working frequency range up to some megahertz [1]–[3]. Terahertz frequency technique has been presented, which requires, however, a complicated and expensive system [4]. Microwave probe pumping techniques [5], [6] are also a promising technique, which uses microwave frequencies. These techniques generally use a scanning process and suffer from the low signal-to-noise ratio due to the spread of induced field in the strong anisotropic medium.

In this paper, a new method based on the induction thermography technique [7]–[9] is proposed in order to characterize the electrical conductivities of anisotropic materials. Because of the strong dependence of inductive electromagnetic power density distribution on the anisotropy ratio, the temperature image (the thermal effect of electromagnetic phenomena recorded by the infrared thermal camera) can be used to better observe the dispersion of induced electromagnetic field in the anisotropic material. A coupled and fully anisotropic electromagnetic-thermal model is developed to simulate the process. This model is based on hexahedral elements to model thin regions of anisotropic physical properties [10]. Eddy-current problem is solved using the $\boldsymbol{T}$-Ω formulation as a fast numerical model.

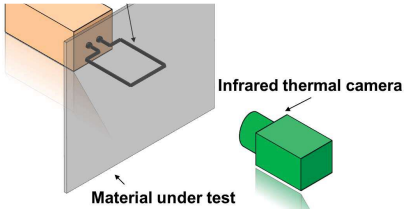

Fig. 1. Induction thermography setup.

Section II presents the technique used. The numerical model is introduced in Sections III and IV. Section V gives the algorithm for identification of the electrical resistivity tensor of CFRP. Identification result is shown in Section VI. Finally, the impact of the anisotropy on the electromagnetic and thermal responses of the unidirectional CFRP is investigated in Section VII by means of the numerical model.

II. Induction Thermography Technique

Fig. 1 shows an induction thermography testing setup. The specimen is heated by means of a U-shaped coil, which is fed by an induction generator via an impedance adaptation circuit. The specimen is heated up to 20 °C above the ambient temperature. The time evolution of the temperature on the surface of the specimen is then recorded. The latter is then used as the input of an error minimization algorithm to identify the electrical resistivity tensor that allows for the best reconstruction of the measured temperature image. It will be shown, in the next sections, that the induced power, and therefore the temperature level, and the pattern of temperature images depend strongly on the anisotropy ratio of the material.

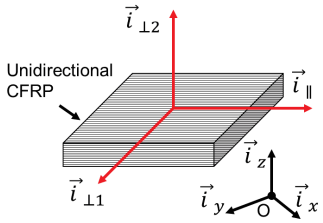

Fig. 2. Local coordinate $(\vec{i}_{\parallel}, \vec{i}_{\perp 1}, \vec{i}_{\perp 2})$ related to fiber direction and global coordinate $(\vec{i}_x, \vec{i}_y, \vec{i}_z)$.

III. T-Ω Formulation for Anisotropic Materials

The matrix form of the discrete T-Ω formulation for fully anisotropic material reads

$$\begin{aligned}\left(\mathbf{R}^t \mathbf{M}_{ff}^{[\rho^e]} \mathbf{R} + j\omega \mathbf{M}_{ee}^{[\mu]}\right) \boldsymbol{T}_e - j\omega \mathbf{M}_{ee}^{[\mu]} \mathbf{G} \Omega_n \\ = -\mathbf{R}^t \mathbf{M}_{ff}^{[\rho^e]} \mathbf{R} \boldsymbol{H}_e^s - j\omega \mathbf{M}_{ee}^{[\mu]} \boldsymbol{H}_e^s \quad (1)\\ -j\omega \mathbf{G}^t \mathbf{M}_{ee}^{[\mu]} \boldsymbol{T}_e + j\omega \mathbf{G}^t \mathbf{M}_{ee}^{[\mu]} \mathbf{G} \Omega_n \\ = j\omega \mathbf{G}^t \mathbf{M}_{ee}^{[\mu]} \boldsymbol{H}_e^s \quad (2)\end{aligned}$$

where $\mathbf{R}$ and $\mathbf{G}$ are, respectively, the discrete counterparts of *rot* and *grad* operators, $\boldsymbol{T}_e = \sum_{i=1}^{E} \mathbf{w}^{e_i} \boldsymbol{T}_e^i$, $\Omega_n = \sum_{i=1}^{N} w^{n_i} \Omega_n^i$, and $\boldsymbol{H}_e^s$ the circulations of the magnetic source field $\boldsymbol{H}^s$ calculated on the edges of the mesh. The components of the matrices $\mathbf{M}_{ff}^{[\rho^e]}$ and $\mathbf{M}_{ee}^{[\mu]}$ are given as follows:

$$\mathbf{M}_{ff}^{[\rho^e]}(i,j) = \sum_k \int_{V_e^k} ((\mathbf{w}^{f_i})^t [\rho^e] \mathbf{w}^{f_j}) dV \quad (3)$$

$$\mathbf{M}_{ee}^{[\mu]}(i,j) = \sum_k \int_{V_e^k} ((\mathbf{w}^{e_i})^t [\mu] \mathbf{w}^{e_i}) dV \quad (4)$$

where t denote the transpose operator. The facet shape functions and the edge shape functions are denoted as $\mathbf{w}^f$ and $\mathbf{w}^e$, respectively. The electrical resistivity tensor and the permeability tensor are denoted as $[\rho^e]$ and $[\mu]$, respectively. The three components of the electrical resistivity of a unidirectional composite ply are denoted as $\rho_{\parallel}^e$, $\rho_{\perp 1}^e$, and $\rho_{\perp 2}^e$, which are, respectively, the homogenized electric resistivity in the fiber axis, perpendicular to the fiber axis and in the normal direction of ply surface as shown in Fig. 2.

Let $\mathbf{T}_{l \to g}$ be the coordinate transformation matrix from local coordinates $(\vec{i}_{\parallel}, \vec{i}_{\perp 1}, \vec{i}_{\perp 2})$ to global coordinates $(\vec{i}_x, \vec{i}_y, \vec{i}_z)$. For any vector $\vec{J}$, its global coordinate $\vec{J}_g$ can be calculated from the local one as

$$\vec{J}_g = \mathbf{T}_{l \to g} \vec{J}_l. \quad (5)$$

The tensor of physical properties in the global coordinates can be obtained as follows:

$$[\rho^e] = \mathbf{T}_{l \to g} \begin{pmatrix} \rho_{\parallel}^e & 0 & 0 \\ 0 & \rho_{\perp 1}^e & 0 \\ 0 & 0 & \rho_{\perp 2}^e \end{pmatrix} \mathbf{T}_{l \to g}^t. \quad (6)$$

Note that, in the case of CFRP, $\rho_{\perp 1}^e = \rho_{\perp 2}^e$.

IV. Thermal Problem

The considered heat source is the eddy-current losses in the composite, whose volume density can be determined by $P = \widehat{\boldsymbol{J}}([\rho^e].\boldsymbol{J})$, where $\widehat{\boldsymbol{J}}$ is the complex conjugate of eddy-current density $\boldsymbol{J}$. The matrix form of thermal weak formulation reads

$$\left(\mathbf{M}_{nn}^{[\rho C]} + \boldsymbol{G}^t \mathbf{M}_{ee}^{[\lambda]} \boldsymbol{G} + \mathbf{M}_{nn}^{[h]}\right) \Delta T_{n,i+1} = \mathbf{M}_n^{[P]} + \mathbf{M}_{nn}^{[\rho C]} \Delta T_{n,i} \quad (7)$$

where $\Delta T_{n,i}$ is the temperature rise on the node n at the instant j with respect to the initial temperature. The matrices $\mathbf{M}_{nn}^{[\rho C]}$, $\mathbf{M}_{ee}^{[\lambda]}$, $\mathbf{M}_{nn}^{[h]}$, and $\mathbf{M}_n^{[P]}$ can be calculated as follows:

$$\mathbf{M}_{nn}^{[\rho C]}(i,j) = \sum_k \int_{V^k} \frac{\rho C_p}{\Delta t} w^{n_i} w^{n_j} dV \quad (8)$$

$$\mathbf{M}_{ee}^{[\lambda]}(i,j) = \sum_k \int_{V^k} (\mathbf{w}^{e_i})^t [\lambda] \mathbf{w}^{e_j} dV \quad (9)$$

$$\mathbf{M}_{nn}^{[h]}(i,j) = \sum_l \int_{S^l} h w^{n_i} w^{n_j} dS \quad (10)$$

$$\mathbf{M}_n^{[P]}(i) = \sum_k \int_{V^k} w^{n_i} P dV. \quad (11)$$

The time step Δt is fixed. $[\lambda]$ is the tensor of thermal conductivity of the material which depends on $\lambda_{\parallel}$, $\lambda_{\perp 1}$, and $\lambda_{\perp 2}$ and can be calculated as in (6). The parameter h takes into account the natural convection and the radiation on the surface of the plate, i.e., $h = h_{\text{conv}} + h_{\text{radi}}$. The heat exchange surface density by natural convection can be estimated by [11]

$$h_{\text{conv}} = N_u \cdot \lambda_{\text{air}} / L \quad (12)$$

where λ_{air} is the thermal conductivity of air in the vicinity of the surface, L is the length of the plate, and N_u is the Nusselt number. The heat exchange surface density by radiation can be calculated as

$$h_{\text{radi}} = \sigma \epsilon \cdot \left(T_{\Gamma^c}^2 + T_0^2\right) \cdot (T_{\Gamma^c} + T_0) \quad (13)$$

where σ is the Stefan–Boltzmann constant, ϵ is the emissivity of the material, T_0 is the room temperature, and T_{Γ^c} is the temperature on the surface of the plate.

V. Algorithm for Identification of the Electrical Resistivity Tensor

We assume that the electrical resistivity is homogenous in the material. For CFRP material, the electric resistivity in the fiber axis can be accurately estimated as function of the filling rate r (in %) of carbon fiber in the composite and the resistivity of carbon fiber ρ_C^e

$$\rho_{\parallel}^e = \frac{\rho_C^e}{r}. \quad (14)$$

With thermal properties of the material given, we search for an identification algorithm to determine the component $\rho_{\perp}^e$ of the electrical resistivity tensor. In addition, the air-gap thickness e is an important factor that should be taken into account. Error in the air-gap measurement may lead to large deviation in the identification. In order to correct this fact, we include the air-gap thickness as identification parameter in the algorithm.

A mono-objective optimization algorithm is used to find the couple $(\rho_{\perp}^e, e)$, which allows for the best fitting of the measured temperature image. The optimization algorithm uses the coupled electromagnetic/thermal finite element model to estimate the temperature distribution. The details of the

Input: Image of temperature measured at a given time.
Output: $\rho^e_\perp$ and e

Initialisation :
Set the expected value ϵ of the error objective function.
Calculate $\rho^e_\parallel$ by using (14).
Initialize $\rho^e_\perp$ and e.
Compute $\mathbf{M}^{[\rho^e]}_{ff}$, $\boldsymbol{H}^s_e$ and $\mathbf{M}^{[\mu]}_{ee}$.
Compute $\mathbf{M}^{[\rho C]}_{nn}$, $\mathbf{M}^{[\lambda]}_{ee}$ and $\mathbf{M}^{[h]}_{nn}$.
Error Minimization Process

while The number of iterations $k < MAX_g$ **do**
  Solve the system (1) and (2).
  Compute $\boldsymbol{J} = \mathbf{R}(\boldsymbol{T}_e + \boldsymbol{H}^s_e)$ and $P = \widehat{\boldsymbol{J}}\,([\rho^e].\boldsymbol{J})$.
  Compute $\mathbf{M}^{[P]}_n$.
  Solve the system (7).
  Compute the error objective function f_e using (15).
  if $MIN(f_e) > \epsilon$ **then**
    Generate a new couple $(\rho^e_\perp, e)$.
    Compute $\mathbf{M}^{[\rho^e]}_{ff}$ and $\boldsymbol{H}^s_e$.
    Update (1) and (2).
  else
    return The best $(\rho^e_\perp, e)$ found.
  end if
end while
return The best $(\rho^e_\perp, e)$ found.

Fig. 3. Algorithm to determine the $\rho^e_\perp$ component of CFRP using an optimization method.

algorithm are given in Fig. 3. The following error objective function can be used in the algorithm:

$$f_e = \sqrt{\sum \left(\Delta T^{\text{sim}}_{(i,j)} - \Delta T^{\text{mes}}_{(i,j)}\right)^2} \qquad (15)$$

where ΔT^{mes} and ΔT^{sim} are, respectively, the measured and simulated temperature image at a given time.

VI. Identification Result

A. Measurement

The measurement setup is shown in Fig. 1. The specimen is a unidirectional CFRP plate, whose overall dimension is 400 mm × 300 mm × 1.92 mm. A U-shaped inductor, as shown in Fig. 1, is used. The CFRP plate is heated during 5 s with an excitation current $I_{\text{exc}} = 324$ A and with a frequency f of 1645 kHz. The measured air gap is about 5 mm. An FLIR SC655 infrared camera with a spectral range of 7.5–13 μm is used to record the temperature at 50 Hz rate. The camera has a thermal sensitivity lower than 50 mK. The surface of the material is painted using black paint with homogeneous emissivity of 0.9. The temperature image obtained at the end of the heating phase (end of electromagnetic excitation) at 5 s is shown in Fig. 4(a). The time evolution of the temperature at some points is shown in Fig. 4(b). For instant, only one temperature image at the end of the heating phase is used as ΔT^{mes} in the error objective function (15). It is noted that more complex objective functions making use of various temperature image sequences [12] could also be used in order to improve the accuracy of the method.

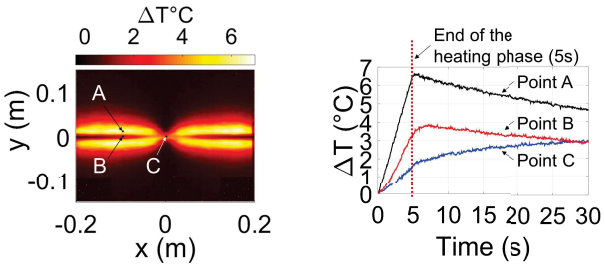

(a) (b)

Fig. 4. Measurement results of the temperature obtained on a unidirectional CFRP. (a) Temperature image at 5 s. (b) Time evolution of the temperature.

TABLE I
Entry Parameters of the Nelder–Mead Simplex Algorithm

Parameter	Value	Unit
Maximal number of iteration	15	-
$\rho^e_\parallel$	25 ($r = 60\%$)	$\mu\Omega \cdot m$
Starting value of $\rho^e_\perp$	10^6 ($r_a = 400000$)	$\mu\Omega \cdot m$
Starting value of e	5 (measured)	mm

TABLE II
Thermal Parameters

Parameter	Value	Unit
ρ	1600	kg/m^3
C_p	900	$J/(kgK)$
$\lambda_\parallel$	4.17	$W/(mK)$
$\lambda_\perp$	0.48	$W/(mK)$
$h = h_{conv} + h_{radi}$	12	Wm^2K

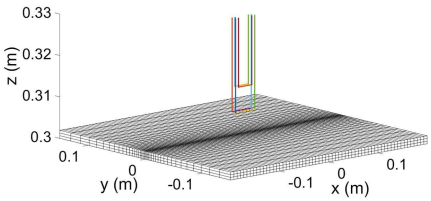

Fig. 5. Mesh with three layers along the thickness. The frame of the inductor is shown above.

TABLE III
Result of the Identification

Best value of f_e	43.6
$\rho^e_\perp (\mu\Omega \cdot m)$	$17.81 \cdot 10^4$ ($r_a = 7124$)
$e(mm)$	5.33
P_{total} (W)	66.12
Total computation time (hours)	1.12

B. Result

The results of the identification method are given in this section. A Nelder–Mead simplex method-based algorithm is used [13]. Some entry parameters of the algorithm are shown in Table I. Thermal parameters are given in Table II [14]. The mesh used in the simulation is shown in Fig. 5. The results of the parameter identification method are given in Table III. The convergence history is shown in Fig. 6.

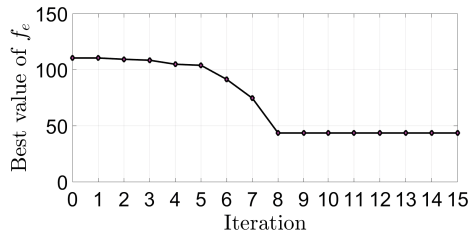

Fig. 6. Convergence history of the Nelder–Mead simplex algorithm.

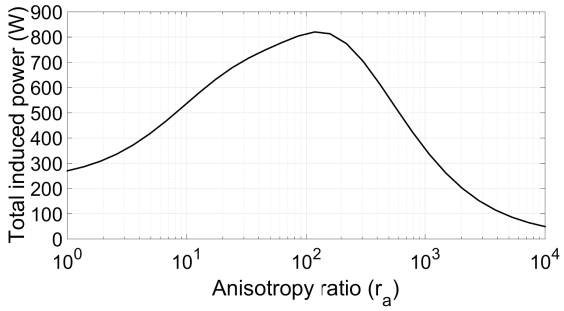

Fig. 7. Variation of total induced power as function of the ratio of anisotropy r_a (note that the r_a-axis is in logarithmic scale).

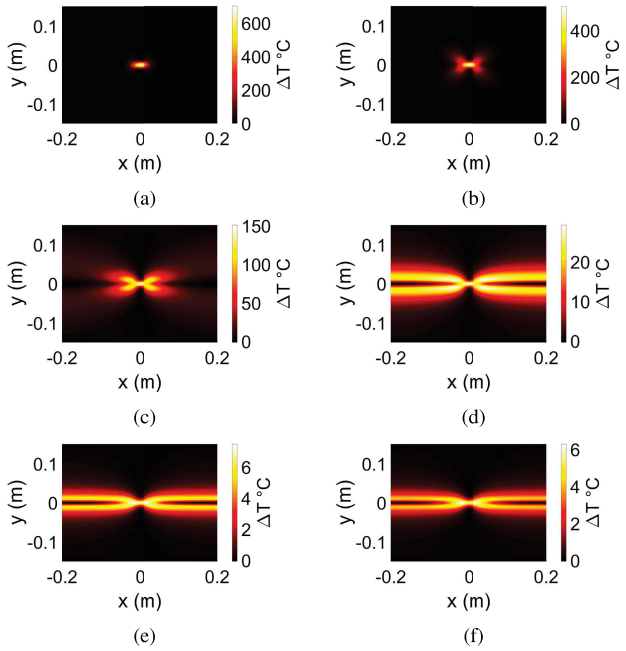

Fig. 8. Temperature image obtained at the end of the heating phase. (a) $r_a = 1$ and $\rho^e_\perp = 25\ \mu\Omega\cdot$m. (b) $r_a = 10$ and $\rho^e_\perp = 250\ \mu\Omega\cdot$m. (c) $r_a = 100$ and $\rho^e_\perp = 2500\ \mu\Omega\cdot$m. (d) $r_a = 1000$ and $\rho^e_\perp = 25\,000\ \mu\Omega\cdot$m. (e) $r_a = 7124$ and $\rho^e_\perp = 178\,100\ \mu\Omega\cdot$m. (f) $r_a = 10\,000$ and $\rho^e_\perp = 250\,000\ \mu\Omega\cdot$m.

VII. Some Simulation Investigations

In this section, we investigate the influence of the anisotropy on the electromagnetic and thermal responses of the unidirectional CFRP. Simulations are carried out with various anisotropy ratio r_a, which is defined as $r_a = (\mathrm{MAX}(\rho^e_{\perp 1}, \rho^e_{\perp 2})/\rho^e_\parallel)$. For isotropic materials, $r_a = 1$. In the simulations, $\rho^e_\parallel$ is fixed to 25 $\mu\Omega\cdot$m and $\rho^e_{\perp 1} = \rho^e_{\perp 2} = \rho^e_\perp \geq \rho^e_\parallel$. In this case, one can define two skin depths according, respectively, to two resistivities: $\delta_\parallel = (\rho^e_\parallel/\pi f \mu_0)^{1/2}$ and $\delta_\perp = (\rho^e_\perp/\pi f \mu_0)^{1/2}$. At given frequency (1645 kHz), $\delta_\parallel$ is equal to 0.62 mm and inversely proportional to $\delta_\perp$ by the factor $\sqrt{r_a}$. The excitation current and the air-gap thickness are, respectively, $I_{\mathrm{exc}} = 324$ A and $e = 5.33$ mm. Fig. 7 shows the variation of the total power induced in the test piece with respect to various ratios of anisotropy. The figure shows a strong dependence of power on the anisotropy. Maximum power can be obtained with r_a between 100 and 150 and decreases rapidly outside this range.

Fig. 8 shows the temperature of the material for various anisotropy ratios. It is clearly shown that the temperature image patterns are strongly related to the ratio of anisotropy. As can be seen, in the case of strongly anisotropic material as CFRP, simulation results give a good accordance with measurement.

VIII. Conclusion

A method to identify the tensor of electrical conductivity of the CFRP was presented. The method can give a good idea about the ratio of anisotropy of the material due to its strong correlation with the temperature distribution. In the further work, the method can be applied to multi-directional CFRP. The temperature evolution in the cooling phase (decrease of temperature after heat excitation) would be exploited to identify thermal properties of the material.

References

[1] M. P. De Goeje and K. E. D. Wapenaar, "Non-destructive inspection of carbon fibre-reinforced plastics using eddy current methods," *Composites*, vol. 23, no. 3, pp. 147–157, 1992.

[2] R. Lange and G. Mook, "Structural analysis of CFRP using eddy current methods," *NDT & E Int.*, vol. 27, no. 5, pp. 241–248, 1994.

[3] G. Mook, R. Lange, and O. Koeser, "Non-destructive characterisation of carbon-fibre-reinforced plastics by means of eddy-currents," *Composites Sci. Technol.*, vol. 61, no. 6, pp. 865–873, 2001.

[4] K. H. Im, D. K. Hsu, C. P. Chiou, D. J. Barnard, I. Y. Yang, and J. W. Park, "Terahertz radiation study on FRP composite solid laminates," in *Proc. AIP Conf.*, 2012, vol. 1430. no. 31, pp. 1192–1199.

[5] H. Lee *et al.*, "Characterization of anisotropic electrical conductivity of carbon fiber composite materials by a microwave probe pumping technique," *J. Composite Mater.*, vol. 50, no. 15, pp. 1999–2004, 2016.

[6] Z. Li and Z. Meng, "A review of the radio frequency non-destructive testing for carbon-fibre composites," *Meas. Sci. Rev.*, vol. 16, no. 2, pp. 68–76, 2016.

[7] H. K. Bui, G. Wasselynck, D. Trichet, B. Ramdane, G. Berthiau, and J. Fouladgar, "3-D modeling of thermo inductive non destructive testing method applied to multilayer composite," *IEEE Trans. Magn.*, vol. 49, no. 5, pp. 1949–1952, May 2013.

[8] H. K. Bui, G. Wasselynck, D. Trichet, and G. Berthiau, "Study on flaw detectability of NDT induction thermography technique for laminated CFRP composites," *Eur. Phys. J. Appl. Phys. (EPJ AP)*, vol. 73, no. 1, p. 10902, 2016.

[9] B. Gao, W. L. Woo, and G. Y. Tian, "Electromagnetic thermography nondestructive evaluation: Physics-based modeling and pattern mining," *Sci. Rep.*, vol. 6, p. 25480, Oct. 2015.

[10] H. K. Bui, G. Wasselynck, D. Trichet, and G. Berthiau, "Performance assessment of induction thermography technique applied to carbon-fiber-reinforced polymer material," *IEEE Trans. Magn.*, vol. 51, no. 3, Mar. 2015, Art. no. 8001804.

[11] A. Bejan and A. D. Kraus, Eds., *Heat Transfer Handbook*. Hoboken, NJ, USA: Wiley, 2003.

[12] C. Ibarra-Castanedo, D. González, M. Klein, M. Pilla, S. Vallerand, and X. Maldague, "Infrared image processing and data analysis," *Infr. Phys., Technol.*, vol. 46, nos. 1–2, pp. 75–83, Dec. 2004.

[13] *MATLAB Documentation (Fminsearch Functions)*, MathWorks., Natick, MA, USA, 2017.

[14] C. Ageorges, L. Ye, Y.-W. Mai, and M. Hou, "Characteristics of resistance welding of lap shear coupons. Part I: Heat transfer," *Composites A*, vol. 29, no. 98, pp. 899–909, 2006.